Dynamics of Kuramoto oscillators with time-delayed positive and negative couplings

Hui Wu[1] and Mukesh Dhamala[2]

[1]*Department of Mathematics, Clark Atlanta University, Atlanta, Georgia 30314, USA*
[2]*Department of Physics and Astronomy, Neuroscience Institute, Georgia State and Georgia Tech Center for Advanced Brain Imaging, Georgia State University, Atlanta, Georgia 30303, USA*

Many real-world examples of distributed oscillators involve not only time delays but also attractive (positive) and repulsive (negative) influences in their network interactions. Here, considering such examples, we generalize the Kuramoto model of globally coupled identical oscillators with time-delayed positive and negative couplings to explore the effects of such couplings in collective phase synchronization. We analytically derive the exact boundaries for stable incoherent and coherent states in terms of the system parameters allowing us to examine the interplay of symmetric and asymmetric time delays and couplings in collective synchronization. Dependent on these parameters, regions of coherent, incoherent, and mixed (coherent, partially coherent, incoherent) states with hysteresis are possible. The region of stability for incoherent states decreases with increasing time delay in all cases and it overall gets reduced in the presence of a time delay in repulsive coupling. The time-delay effects for instability can become more significant at the delay values that are about half an oscillation period length, or its multiples in the case of positive time-delay couplings, and is about a full period or its multiples in case of negative delayed couplings. The mixed state region shows multistability among fully coherent, fully incoherent, and partially coherent (clustered) states. Partially coherent or clustered states occur near the instability-stability boundaries and can show quasiperiodic and nonstationary behaviors. We discuss the implications of the model and the results for natural systems, particularly neuronal network systems in the brain.

I. INTRODUCTION

The Kuramoto model [1], originally formulated to simplify Winfree's biological oscillator model for the circadian rhythms of living systems [2], represents an analytically tractable model to study collective synchronization in large systems of coupled nonlinear oscillators. Since its conception, the Kuramoto model has been generalized to explain collective dynamical behaviors in many natural and technological systems of coupled nonlinear oscillators often with various coupling scenarios [3–6]. As nature is replete with beautiful complexities such as self-organized critical phenomena [7] arising from opposing forces, the interplay of positive-negative time-delayed interactions in the Kuramoto model of oscillators can also be expected to show rich dynamical behaviors yet to be investigated.

The generalizations of the Kuramoto model previously analyzed include coupling scenarios with separate time-delayed interactions, and positive as well as negative coupling. In an outstanding analytical work, Yeung and Strogatz [8] considered time delay in a mean-field sinusoidal coupling of the Kuramoto model and derived exact formulas for the stability boundaries of the incoherent and synchronized states as a functional of the delay in a special case where the oscillators were identical. Later, Earl and Strogatz [9] extended the analysis to a variety of coupling topologies (regular, small-world, and random network graphs) to find that the same stability criterion held true as for the mean-field case. In another more recent study, Hong and Strogatz [10,11] studied the Kuramoto model with positive and negative coupling

parameters (without time delay) and reported a variety of dynamical behaviors including fully synchronized, partially synchronized, desynchronized, and traveling states. Qui and colleagues [12] recently discovered a new nonstationary state (named *Bellerophone*) along with a synchronized state in the model with positive and negative coupling. In networks of globally coupled Kuramoto oscillators with attractive and repulsive couplings (similar to networks of excitatory and inhibitory neurons), Maistrenko and colleagues discovered solitary states as a dynamical mechanism for desynchronization [13]. Petkoski and colleagues recently analytically studied the regions of stability for phase synchronization in networks of Kuramoto oscillators with bimodally distributed time delays in positive coupling [14]. However, the dynamics of the Kuramoto model with combined time-delayed interactions and positive-negative (attractive-repulsive or excitatory-inhibitory) couplings have largely remained unexplored despite their relevance to many natural systems, such as biological, physical, chemical, and social networks.

Interaction time delays and excitation-inhibition (E-I) are usually characteristics of spatially distributed, self-organized systems, such as neurons in the brain in which the E-I balance is required to maintain normal temporal and spatial functional organization in healthy cognitive functions and behaviors [15–19]. Networks of coupled excitatory and inhibitory neurons can exhibit a complex dynamical behaviors including synchronization, multiclustered solutions, and oscillator death [20]. E-I couplings in Belousov-Zhabotinsky can lead to a large number of spatiotemporal patterns, simple to complex

behaviors [21]. In social networks of conformists (dynamical units with positive coupling) and contrarians (those with negative coupling) also, various collective behaviors are possible [11,22,23]. Interactions in spatially distributed oscillator network systems are not generally instantaneous. On the contrary, finite speed of signal transmission over a distance gives rise to a finite time delay. For example, signal transmission time delays are inherent in networks of neurons in the brain. While the chemical synaptic time delays are small (∼2 ms), the axonal conduction delays, which depend on the distance between neurons in the brain, can reach up to tens of milliseconds [24]. Time delays comparable to timescales of neuronal oscillations are known to have significant effects in the collective (ensemble) activity of neurons [24–26]. Time delays in networks of coupled inhibitory neurons can induce a variety of phase-coherent dynamic behaviors, including completely coherent, partially coherent, and periodic patterns [27]. Time delays in networks with E-I can be expected to induce a variety of collective dynamical behaviors, such as coherent, partially coherent, and multistable states.

In this work, we analyze a generalized Kuramoto model of nonlinear oscillators with time-delayed positive and negative couplings for stability of coherent and incoherent states, and derive the exact analytical solutions to define the parameter boundaries for these states. As a general result, we come to show that fully coherent, incoherent states and mixed (coherent, incoherent, and clustered) states are possible, and that the system commonly displays these states and other complex behaviors in cases of symmetric and asymmetric time delays in positive and negative couplings.

II. METHODS AND RESULTS

We start with the following generalized Kuramoto model of N oscillators globally connected with time-delayed positive and negative couplings:

$$\dot{\theta}_i(t) = \omega_0 + \frac{k_1}{N_1} \sum_{j=1}^{N_1} f[\theta_j(t - \tau_{ji}) - \theta_i(t)]$$

$$+ \frac{k_2}{N_2} \sum_{j=N_1+1}^{N} f[\theta_j(t - \tau_{ji}) - \theta_i(t)]. \quad (1)$$

Here the coupled system consists of N_1 and N_2 numbers of positively and negatively coupled oscillators. The total number is $N = N_1 + N_2$, and $k_1 + k_2 = (1 - c)k$. $k_1 = k > 0$ is a positive coupling strength, $k_2 < 0$ is a negative coupling strength, and $c = -k_2/k = |k_2|/k$ is the coupling ratio. $\theta_i(t)$ is the phase of the ith oscillator, $\dot{\theta}_i(t)$ its derivative, and each oscillator has the same natural frequency w_0. f is a general coupling function, which we replace with a sinusoidal function in our examples below. τ_{ji} is the overall time delay for a signal to go from oscillator j to oscillator i, which includes internal node-level intrinsic processing time plus the time for the signal transfer along the pathway. Here we further assign τ_{ji} to be τ_1 for the time delay associated with positive coupling and τ_2 for the time delay with negative coupling. Figure 1 illustrates with a five-oscillator network the type of coupled oscillator system described by Eq. (1). Notice that
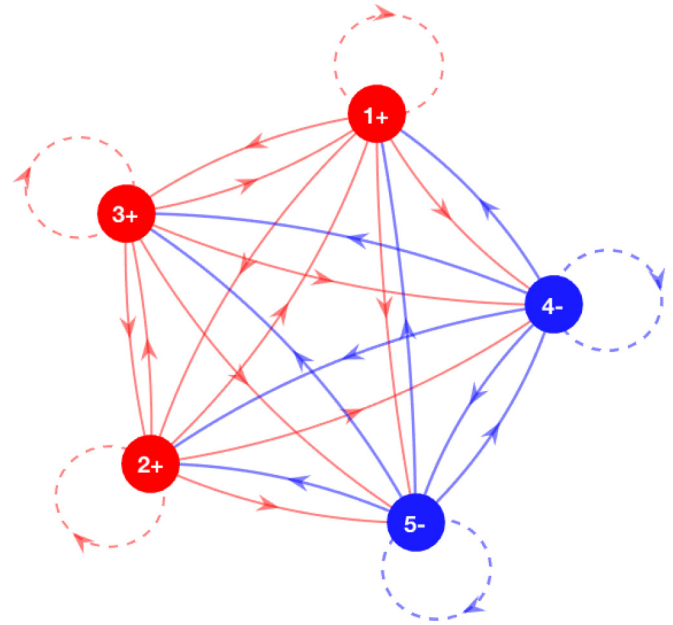

FIG. 1. A schematic of a network of all-to-all coupled oscillators (filled circles) with time-delayed positive and negative interactions (lines with arrows). Equation (1) represents such a network with infinitely large number of oscillators ($N_1 \to \infty$ and $N_2 \to \infty$, the thermodynamic limit). Here, we use only five oscillators for a simpler illustration of the network structure. Red filled circles represent the network nodes that send positive couplings (red edges) to all others, and blue circles represent those that send negative couplings (blue edges). The time delay from a red node to a blue node is τ_1 and the other way around is τ_2. In our analysis of the generalized Kuramoto model [Eq. (1)], we consider the cases of symmetric ($\tau_1 = \tau_2$) and asymmetric ($\tau_1 \neq \tau_2$, one of them being zero) time delays between oscillators. The effect of self-coupling (dashed line) becomes negligible in the thermodynamic limit.

this network structure with positive and negative couplings is different from the one used in [10] but is consistent with the notion of networks of excitatory and inhibitory neurons studied in neuroscience. The overall time delays in the neuronal circuits in the brain depend on intrinsic processing and axonal conduction time, which can be different for excitatory and inhibitory neurons [28]. Below, we consider the cases of symmetric ($\tau_{ji} = \tau_{ij}$) and asymmetric ($\tau_{ji} \neq \tau_{ij}$) time delays between positively and negatively coupled oscillators and explore the interplay of the parameters (k, c, τ_1, and τ_2) in the emergence of stable coherent states.

The rest of the paper is organized as follows: (a) we analyze the stability of a completely coherent state and derive the boundary curves for the coherent state, (b) we analyze the stability of a completely incoherent state and derive the boundary curves for the incoherent state. In each case, we consider the following scenarios of delays: (i) $\tau_1 = \tau_2 = \tau$, and (ii) $\tau_1 = \tau > 0$ and $\tau_2 = 0$, (iii) $\tau_1 = 0$ and $\tau_2 = \tau > 0$. For the first case (a), we analyzed the time evolution of a perturbation to a synchronized state. For the second case (b), we linearize the continuity equation around the incoherent state [$\rho(\theta, \omega, t) = 1/2\pi$] describing the time evolution of instantaneous phase distribution $\rho(\theta, \omega, t)$ on a unit circle, and analyze the effect of a perturbation to the incoherent state.

A. Stability of coherent state

We assume the system reaches a complete synchronized state described by the following equation:

$$\theta_i(t) = \Omega t. \qquad (2)$$

The collective frequency Ω is given by

$$\Omega = \omega_0 + k_1 f(-\Omega\tau_1) + k_2 f(-\Omega\tau_2). \qquad (3)$$

Now we add a small perturbation term on (2):

$$\theta_i(t) = \Omega t + \epsilon\phi_i(t), \qquad (4)$$

where $0 < \epsilon \ll 1$. Now, if we define $\Delta_i(t) := \phi_i(t) - \phi_1(t)$,

$$
\begin{aligned}
\dot{\Delta}_i(t) &= -\frac{k_1}{N_1} f'(-\Omega\tau_1) \sum_{j=1}^{N_1} \Delta_i(t) \\
&\quad - \frac{k_2}{N_2} f'(-\Omega\tau_2) \sum_{j=N_1+1}^{N} \Delta_i(t) \\
&= -[k_1 f'(-\Omega\tau_1) + k_2 f'(-\Omega\tau_2)]\Delta_i(t). \qquad (5)
\end{aligned}
$$

One of the stability requirements for phase synchronization is that none of the oscillators leave the synchronous cluster [29]. For that, $\Delta_i(t)$ needs to decay to zero instead of diverging to infinity. Hence,

$$k_1 f'(-\Omega\tau_1) + k_2 f'(-\Omega\tau_2) > 0. \qquad (6)$$

When (6) is satisfied $\forall i = 1, 2, 3, \ldots N$, $\phi_i(t)$ exponentially converges to the same function $\phi(t)$. Thus, $\phi(t)$ satisfies the following time-delay equation:

$$
\begin{aligned}
\dot{\phi}(t) &= k_1 f'(-\Omega\tau_1)[\phi(t-\tau_1) - \phi(t)] \\
&\quad + k_2 f'(-\Omega\tau_2)[\phi(t-\tau_2) - \phi(t)]. \qquad (7)
\end{aligned}
$$

If we let $\tau_1 = \tau_2 = \tau$ for a synchronization state, we have

$$
\begin{aligned}
&(1-c)f'(-\Omega\tau) > 0, \\
&\dot{\phi}(t) = (1-c)kf'(-\Omega\tau)[\phi(t-\tau) - \phi(t)]. \qquad (8)
\end{aligned}
$$

With $\phi(t) = e^{\lambda t}$ to find the characteristic function, we have

$$\lambda = (1-c)kf'(-\Omega\tau)(e^{-\lambda\tau} - 1). \qquad (9)$$

Another stability requirement for phase synchronization is that the angular speed Ω be stably uniform [29]. For this, the real part of each eigenvalue needs to be negative. All the eigenvalues of this characteristic function have negative real parts if and only if $(1-c)k\tau f'(\Omega\tau) > -1$, which is already included in Eq. (8). Hence, if Eq. (8) is satisfied, the homogeneous rotation is guaranteed.

We now let the general coupling function to be a sinusoidal, $f(\theta) = \sin(\theta)$, for $\tau_1 = \tau_2 = \tau$ and we arrive at the following two cases: (i) if $1 - c > 0$, then $\cos(\Omega\tau) > 0$, and (ii) if $1 - c < 0$, then $\cos(\Omega\tau) < 0$.

We let $T = \frac{2\pi}{\omega_0}$, $y = \frac{k}{\omega_0}$ and arrive at the solutions for the boundary curves of the unstable coherent states in two cases: (i) when $1 - c > 0$, we have

$$\frac{4n+1}{4[1-(1-c)y]} < \frac{\tau}{T} < \frac{4n+3}{4[1+(1-c)y]}, \qquad (10)$$
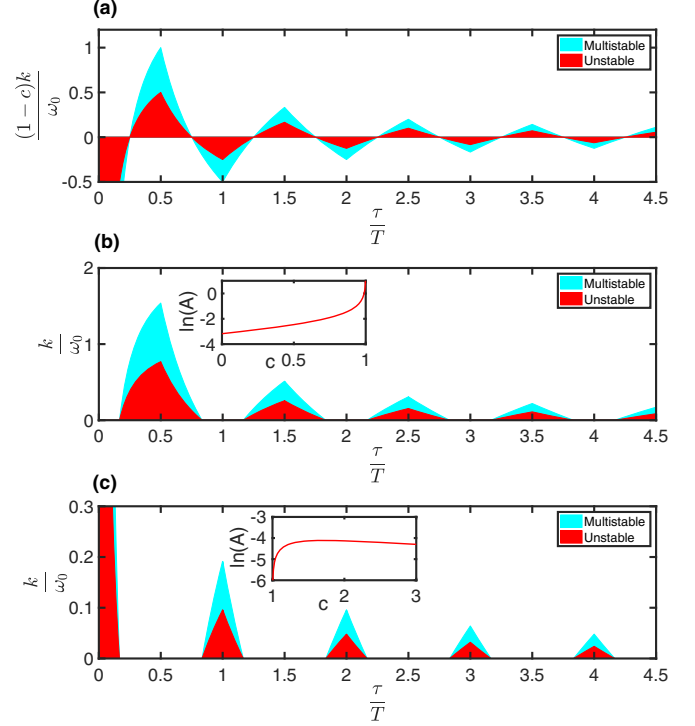

FIG. 2. Regions of unstable coherent and stable incoherent states (red color or darker shade), stable coherent and incoherent states (cyan color or lighter shade), and stable coherent state (unshaded or white) as a function of coupling strength and time delay in cases of symmetric time delays ($\tau_1 = \tau_2$) (a), and asymmetric time delays ($\tau_1 \neq \tau_2$) and $c = 0.5$ in (b), and $c = 2.0$ in (c). Here, the region of the incoherent state becomes progressively smaller with increasing time delay for all cases: unstable area decreases as $1/\tau$. In the case of symmetric time delays [shown in (a)], a stable coherent state exists for dominant negative coupling (coupling ratio, $c > 1$). In the cases of asymmetric time delays, a stable coherent state does not exist for dominant negative coupling ($c > 1$) when time delay is zero in the negative coupling [shown in (b)], and a time delay in the negative coupling and zero delay in the positive coupling [as shown in (c)] further reduces the region of stable incoherent state. The time-delay effects become more significant at delays nearly equal to the half oscillation period or its multiples (locations of boundary peaks in (b)) for time delays present only in positive couplings or at delays equal to a full period or its multiples in case of time delays only present in negative couplings (c). The cyan color (lighter) shaded region can exhibit stable coherent, incoherent, and clustered states, collectively referred to as mixed or multistable states. The insets in (b, c) show how the unstable area (red) [$A \approx \frac{1}{2}W(c)H(c)$ for $n = 1$] varies with the coupling ratio c.

and $0 < y < \frac{1}{2(1-c)(2n+1)}$, and (ii) when $1 - c < 0$, we have

$$\frac{4n-1}{4[1+(1-c)y]} < \frac{\tau}{T} < \frac{4n+1}{4[1-(1-c)y]}, \qquad (11)$$

and $0 < y < \frac{1}{4n(c-1)}$. We use (10) and (11) to draw the boundary curves and areas for unstable synchronized states, as shown in the red color shades of Fig. 2(a).

We now consider $f(\theta) = \sin(\theta)$, $\tau_1 = \tau > 0$, $\tau_2 = 0$, and (6) becomes

$$f'(-\Omega\tau) - cf'(0) > 0. \tag{12}$$

According to (12),

$$\cos(\Omega\tau) - c > 0 \tag{13}$$

is required to have a stable solution. This solution (13) implies that when $\tau_1 = \tau > 0$, $\tau_2 = 0$, in case of a stronger negative coupling ($c > 1$), a stable coherent state does not exist. When $\cos(\Omega\tau) - c > 0$, $\forall i = 1, 2, \ldots N$: $\phi_i(t)$ exponentially converges to the same $\phi(t)$, $\phi(t)$ and then satisfies the following equation:

$$\dot{\phi}(t) = k\cos(\Omega\tau)[\phi(t - \tau) - \phi(t)].$$

Then, for uniform rotation, all eigenvalues need to have negative real parts. The characteristic function thus satisfies

$$\lambda = k\cos(\Omega\tau)(e^{-\lambda\tau} - 1). \tag{14}$$

It is easy to show that for any $k > 0$ and $\cos(\Omega\tau) > c$, for all $\lambda \neq 0$, $\mathrm{Re}(\lambda) < 0$. Therefore, the synchronized state is always linearly stable when (13) is satisfied. Whenever $c \geqslant 1$, we do not have a stable coherent state. Taking $x = \frac{\tau}{T}$, $y = \frac{k}{\omega_0}$, $T = \frac{2\pi}{\omega_0}$, when $0 < c < 1$, the coherent state is unstable if and only if τ satisfies following inequality:

$$\frac{2n\pi + \arccos c}{2\pi(1 - \sqrt{1 - c^2}y)} < \frac{\tau}{T} < \frac{2(n+1)\pi - \arccos c}{2\pi(1 + \sqrt{1 - c^2}y)}. \tag{15}$$

Here, the width and height of the unstable coherent area in nth period are given as follows:

$$W(c) = \frac{1}{\pi}(\pi - \arccos c),$$

$$H(c) = \frac{\pi - \arccos c}{(2n+1)\pi\sqrt{1 - c^2}}. \tag{16}$$

We use (15) to draw the boundary curves and areas for this unstable coherent state, as shown with red color shade in Fig. 2(b).

Now we consider the stability of the coherent state for $\tau_1 = 0$, $\tau_2 = \tau > 0$. For this case, Eq. (6) yields $\cos(\Omega\tau) < \frac{1}{c}$. Equation (7) becomes

$$\dot{\phi}(t) = -ck\cos(\Omega\tau)[\phi(t - \tau) - \phi(t)].$$

The corresponding eigenfunction satisfies

$$\lambda = -ck\cos(\Omega\tau)(e^{-\lambda\tau} - 1). \tag{17}$$

The eigenvalues for this function have all negative real part if and only if

$$\cos(\Omega\tau) < \frac{1}{ck\tau}. \tag{18}$$

Thus we find that a stable coherent state can exist in this case if and only if

$$\cos(\Omega\tau) < \min\left(\frac{1}{c}, \frac{1}{ck\tau}\right). \tag{19}$$

The coherent state will become unstable within the following boundaries:

$$k\tau\sqrt{c^2 - 1} - \arccos\frac{1}{c} < \omega\tau - 2n\pi$$
$$< \arccos\frac{1}{c} - k\tau\sqrt{c^2 - 1}. \tag{20}$$

Setting $x = \frac{\tau}{T}$ and $y = \frac{k}{\omega_0}$, we have $x < \frac{\arccos\frac{1}{c}}{2\pi(1 + \sqrt{c^2 - 1}y)}$ for $n = 0$ and

$$\frac{2n\pi - \arccos\frac{1}{c}}{2\pi(1 - \sqrt{c^2 - 1}y)} < x < \frac{2n\pi + \arccos\frac{1}{c}}{2\pi(1 + \sqrt{c^2 - 1}y)}, \tag{21}$$

where $n = 1, 2, 3, 4, \ldots$. In this case, the width and height of the unstable coherent area in the nth period are given as follows:

$$W(c) = \frac{1}{\pi}\arccos\frac{1}{c},$$

$$H(c) = \frac{\arccos\frac{1}{c}}{2n\pi\sqrt{c^2 - 1}}. \tag{22}$$

We use (21) to draw the boundary curves and areas for this unstable coherent state, as shown with red color shade in Fig. 2(c).

B. Stability of the incoherent state

We now approach the stability of the incoherent state, from Eq. (1), by considering the mean field of positive oscillators and the mean field of negative oscillators in the thermodynamic limit of N being infinitely large:

$$r_1 e^{i\phi_1} = \frac{1}{N_1}\sum_{j=1}^{N_1} e^{i\theta_j},$$

$$r_2 e^{i\phi_2} = \frac{1}{N_2}\sum_{j=N_1+1}^{N_1+N_2=N} e^{i\theta_j}. \tag{23}$$

The conditional probability density function $\rho(\theta, \omega, t)$ satisfies

$$\int_0^{2\pi} \rho(\theta, \omega, t)d\theta = 1. \tag{24}$$

For the complete incoherent state,

$$\rho(\theta, \omega, t) = \frac{1}{2\pi}. \tag{25}$$

For $\forall i = 1, 2, 3, \ldots N$,

$$r_1 e^{i[\phi_1(t-\tau_1) - \theta_i(t)]} = \frac{1}{N_1}\sum_{j=1}^{N_1} e^{i[\theta_j(t-\tau_1) - \theta_i(t)]}. \tag{26}$$

Similarly,

$$r_2 e^{i[\phi_2(t-\tau_2) - \theta_i(t)]} = \frac{1}{N_2}\sum_{j=N_1+1}^{N} e^{i[\theta_j(t-\tau_2) - \theta_i(t)]}. \tag{27}$$

Considering the imaginary part of (26) and (27), we can transfer the dynamical equation in the mean-field form

as

$$\dot{\theta}_i(t) = \omega_i + k_1 r_1 \sin[\theta_j(t - \tau_1) - \theta_i(t)]$$
$$+ k_2 r_2 \sin[\theta_j(t - \tau_2) - \theta_i(t)]. \quad (28)$$

The equation with a perturbation to the incoherent state is then

$$\rho(\theta, \omega, t) = \frac{1}{2\pi} + \epsilon \eta(\theta, \omega, t), \quad (29)$$

with $\epsilon \ll 1$. Here $\eta(\theta, \omega, \tau)$ can be expanded into the following Fourier series:

$$\eta(\theta, \omega, t) = c(\omega, t)e^{i\theta} + c^*(\omega, t)e^{-i\theta} + \eta^\perp(\theta, \omega, t), \quad (30)$$

where $\eta^\perp$ are higher Fourier harmonics. We now look for a type of solution of the form

$$c(\omega, t) = b(\omega)e^{\lambda t}, \quad (31)$$

$$\lambda b(\omega) = -i\omega b(\omega) + \frac{k_1 e^{-\lambda \tau_1}}{2} \int_{-\infty}^{\infty} b(v)g(v)dv$$
$$+ \frac{k_2 e^{-\lambda \tau_2}}{2} \int_{-\infty}^{\infty} b(v)g(v)dv. \quad (32)$$

For identical frequencies, $\omega_i = \omega_0, \forall i = 1, 2, \ldots N$, $g(\omega) = \delta(\omega - \omega_0)$, δ is the Dirac δ function. The eigenvalue λ satisfies the following equation:

$$\lambda + i\omega_0 = \frac{1}{2}(k_1 e^{-\lambda \tau_1} + k_2 e^{-\lambda \tau_2}). \quad (33)$$

When $\tau_1 = \tau_2 = \tau$, $k_1 = k > 0$, $k_2 = -ck < 0$, $c > 0$ is a constant,

$$(1 - c)k = 2(\lambda + i\omega_0)e^{\lambda \tau}. \quad (34)$$

At a critical (bifurcation) point K_c, the eigenvalue λ passes through the imaginary axis $\lambda = Ri$, where R is real number.

From the equation above, $2(\lambda + i\omega_0)e^{\lambda \tau} = 2i(R + \omega_0)[\cos(R\tau) + i\sin(R\tau)]$ has to be a real value. Hence, $\cos(R\tau) = 0$. If we take $R\tau = (-m + \frac{1}{2})\pi$ with $m \in Z$, we have $(1 - c)k = 2(-1)^{m-1}(R + \omega_0)$ and $2\omega_0\tau + (-1)^m (1 - c)k\tau = -2R\tau = 2(m - \frac{1}{2})\pi = (2m - 1)\pi$. Taking $m = 2n + 1$ odd positive integers, we get one boundary for τ:

$$\tau_{c1} = \frac{(4n + 1)\pi}{2\omega_0 - (1 - c)k}. \quad (35)$$

If we take $m = 2n$ or $m = 2(n + 1)$ even positive integers, we get other boundaries for τ:

$$\tau_{c2} = \frac{(4n - 1)\pi}{2\omega_0 + (1 - c)k}, \quad (36)$$

$$\tau_{c3} = \frac{(4n + 3)\pi}{2\omega_0 + (1 - c)k}. \quad (37)$$

Letting $T = \frac{2\pi}{\omega_0}$, $y = \frac{k}{\omega_0}$, for $(1 - c)k = K > 0$ and $\tau_{c1} < \tau < \tau_{c3}$, we have the stable incoherent state within:

$$\frac{4n + 1}{4(1 - \frac{(1-c)y}{2})} < \frac{\tau}{T} < \frac{4n + 3}{4(1 + \frac{(1-c)y}{2})}. \quad (38)$$

For $(1 - c)k = K < 0$, $\tau_{c2} < \tau < \tau_{c1}$, we have the stable incoherent state within:

$$\frac{4n - 1}{4(1 + \frac{(1-c)y}{2})} < \frac{\tau}{T} < \frac{4n + 1}{4(1 - \frac{(1-c)y}{2})}. \quad (39)$$

We now use Eqs. (38) and (39) to draw the boundary curves and areas for this unstable incoherent state, as shown with cyan color (light) shade in Fig. 2(a). For $\tau_1 = \tau > 0$, $\tau_2 = 0$, the eigenvalue λ has to satisfy the following equation:

$$\lambda + i\omega_0 = \frac{1}{2}(k_1 e^{-\lambda \tau} + k_2). \quad (40)$$

If $c \geqslant 1$, let $\lambda = \alpha + iR$, α, R be real,

$$k[e^{-\alpha \tau} \cos(R\tau) - c] = 2\alpha. \quad (41)$$

It is easy to see that when $c > 1$, (41) requires $\alpha < 0$, while when $c = 1$ and $\alpha \geqslant 0$, then the only possibility to satisfy (41) is $\alpha = R = 0$. So the incoherent state is always neutrally stable when $c \geqslant 1$. An unstable incoherent state only possibly exists for $0 < c < 1$. At a bifurcation point, when $\lambda = Ri$, R is real. Substituting it to (40),

$$[2R + 2\omega_0 + k\sin(\tau R)]i = k[\cos(\tau R) - c]. \quad (42)$$
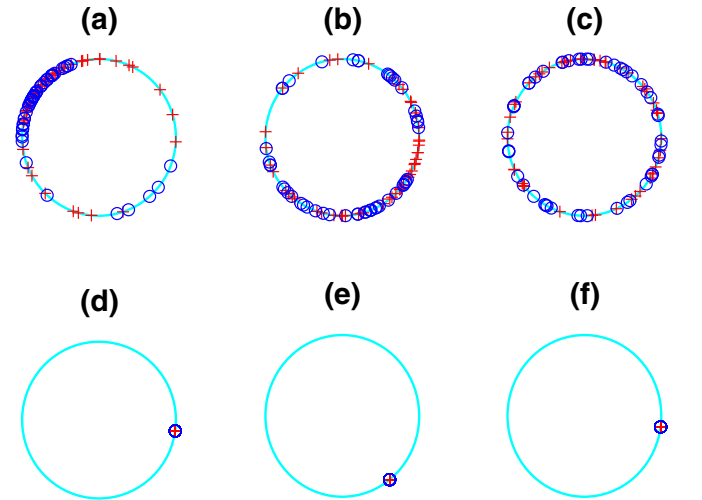

FIG. 3. Examples of incoherent (a, b, c) and coherent (d, e, f) states in cases of symmetric [first column (a, d)] and asymmetric delays [second (b, e) and third (c, f) columns]. The time delay and coupling strength $[x, y]$ coordinates selected from Figs. 2(a)–2(c) for these examples are [0.5, 0.95] for (a), [0.5, 1.025] for (d) [symmetric case from Fig. 2(a)], [0.5, 1.4] for (b), [0.5, 1.6] for (e), [1, 0.16] for (c), [1, 0.22] for (f) [asymmetric cases from Figs. 2(b) and 2(c)]. Here, time-delayed positively and negative coupled phase oscillators are depicted with red plus signs and tiny blue circles, respectively, going around in a big unit circle. The first row shows the asymptotic unsynchronized phase positions of the oscillators from randomly dispersed initial conditions along the circle at coupling strengths and time delays selected from the multistable (cyan color shaded) regions of Figs. 2(a)–2(c). The state of the system in the multistable region depends on the initial conditions: random initial conditions always end up in incoherent states, clustered initial conditions can lead to partially coherent states, and a single cluster initial condition leads to a coherent state. The second row shows that the system even with random initial conditions can transition to coherent states as the coupling strengths are increased out of these multistable regions in all cases of delays (across columns).

The above equation is satisfied if and only if $\cos(\tau R) = c$ and $k \sin(\tau R) = -2(R + \omega_0)$, $\tau R = -2m\pi \pm \arccos c$, m are integers, and $\sin(\tau R) = \pm\sqrt{1-c^2}$, $k = \mp\frac{2(R+\omega_0)}{\sqrt{1-c^2}}$.

If we take $m = n$ and $\tau R = -2n\pi - \arccos c$, we get the left boundary for $\omega_0\tau$ as

$$\omega_0\tau_{lc} = 2n\pi + \arccos c + \tfrac{1}{2}k\tau\sqrt{1-c^2}. \quad (43)$$

Similarly, if take $m = n + 1$ and $\tau R = -2n\pi + \arccos c$, we get the right boundary for $\omega_0\tau$ as

$$\omega_0\tau_{rc} = 2(n+1)\pi - \arccos c - \tfrac{1}{2}k\tau\sqrt{1-c^2}. \quad (44)$$

The incoherent state is stable if and only if $\omega_0\tau_{lc} < \omega_0\tau < \omega_0\tau_{rc}$. If we make $y = \frac{k}{\omega_0}$, we have

$$\frac{2n\pi + \arccos c}{2\pi(1 - \frac{\sqrt{1-c^2}y}{2})} < \frac{\tau}{T} < \frac{2(n+1)\pi - \arccos c}{2\pi(1 + \frac{\sqrt{1-c^2}y}{2})}. \quad (45)$$

We use (45) to draw the boundary curves and areas for this unstable incoherent state, as shown with cyan color (light) shade in Fig. 2(b). When $\tau_1 = 0$, $\tau_2 = \tau > 0$, we have the following characteristic equation of eigenvalue λ:

$$\lambda + i\omega_0 = \frac{k}{2}(1 - ce^{-\lambda\tau}). \quad (46)$$

For $\lambda = iR$ at the bifurcation point along the imaginary axis with real R, we have

$$(R + \omega_0)i = \frac{k}{2}[1 - c\cos(\tau R) + ic\sin(\tau R)]. \quad (47)$$

This equation implies $1 - c\cos(\tau R) = 0$ and $R + \omega_0 = \frac{kc}{2}\sin(\tau R)$. When $\tau R = -2n\pi + \arccos\frac{1}{c}$, $\sin\tau R = \frac{\sqrt{c^2-1}}{c}$, these equations provide one boundary of τ_{lc}:

$$\omega_0\tau_{lc} = 2n\pi - \arccos\frac{1}{c} + \frac{k\tau\sqrt{c^2-1}}{2}. \quad (48)$$

Similarly, when $\tau R = -2n\pi - \arccos\frac{1}{c}$, $\sin\tau R = -\frac{\sqrt{c^2-1}}{c}$, we have another boundary of τ_{rc}:

$$\omega_0\tau_{rc} = 2n\pi + \arccos\frac{1}{c} - \frac{k\tau\sqrt{c^2-1}}{2}. \quad (49)$$

When the incoherent state is stable, τ lies between these two boundaries τ_{lc} and τ_{rc}. Thus we have

$$2n\pi - \arccos\frac{1}{c} + \frac{k\tau\sqrt{c^2-1}}{2} < \omega_0\tau$$
$$< 2n\pi + \arccos\frac{1}{c} - \frac{k\tau\sqrt{c^2-1}}{2}. \quad (50)$$

With $x = \frac{\tau}{T}$ and $y = \frac{k}{\omega_0}$, we have when $n = 0$, $x < \frac{\arccos\frac{1}{c}}{2\pi(1+\frac{\sqrt{c^2-1}y}{2})}$ and for $n = 1, 2, 3, \ldots$,

$$\frac{2n\pi - \arccos\frac{1}{c}}{2\pi(1 - \frac{\sqrt{c^2-1}y}{2})} < x < \frac{2n\pi + \arccos\frac{1}{c}}{2\pi(1 + \frac{\sqrt{c^2-1}y}{2})}. \quad (51)$$

We use (51) to draw the boundary curves and areas for this unstable incoherent state, as shown with cyan color (light) shade in Fig. 2(c).
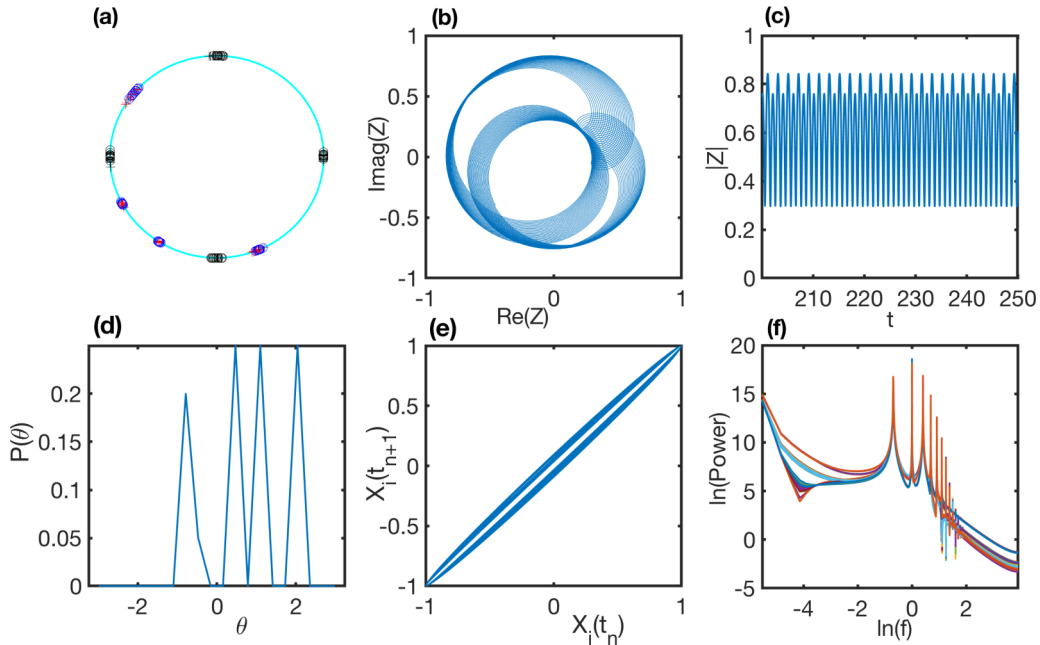

FIG. 4. Example of a clustered state in the multistable region at $[x = 0.5, y = 0.825]$ from Fig. 2(a) and its temporal dynamics. (a) Here the system starts with clustered initial conditions (shown with black $+$ signs and tiny black circles) from four quadrants of a big circle and ends up in four clusters (shown with red $+$ signs and tiny blue circles), where $+$ refers to an oscillator that sends a time-delayed positive coupling to others, and $\circ$ the one that sends time-delayed negative coupling. The final state is a cluster state, as also seen in phase distribution $P(\theta)$ of the final state (d). The temporal behaviors of the system are nonstationary (with time-varying order parameter $[r(t) = |Z(t)|$, where $Z(t) = \sum_j^N \exp(i\theta_j(t))]$ as plotted in (b), (c)] and the trajectory of $X_i(t) = \cos(\theta_i(t))$ resembles quasiperiodic orbit (b, e) with multifrequency power spectra of $X(t)$ (f).
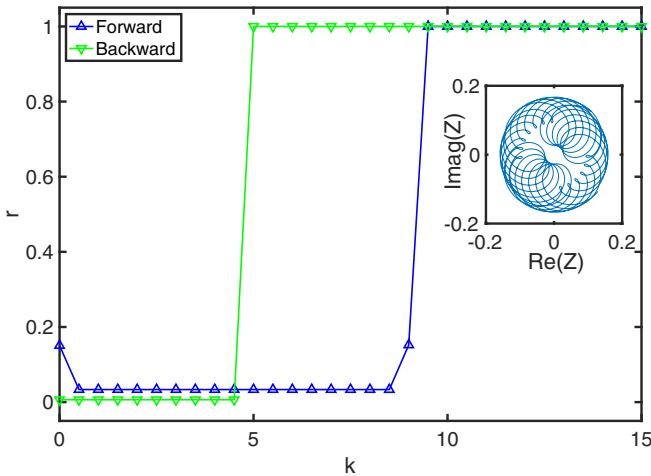
FIG. 5. Abrupt transition to synchrony, hysteresis, and complex temporal behavior. Here, we show an example [for the case ($\tau_1 = 0.5$, $\tau_2 = 0$, $c = 0.5$) of Fig. 2(b)] of abrupt (first-order-like) transitions to synchrony with order parameter [$r = \langle |Z| \rangle$, where $Z(t) = \sum_j^N \exp(i\theta_j(t))$, $\langle . \rangle$ = time average] in the forward (blue) and backward (green) directions of changing coupling strength (k). The presence of two (red and cyan shaded) regions in Figs. 2(a)–2(c) implies that there are hysteresis effects. Near the transition to synchrony (for example, at $k = 9$ for the forward direction), the system starting with random initial conditions shows nonstationary behavior and the trajectory resembles a quasiperiodic orbit (the trajectory of the complex order parameter shown in the inset).

C. Numerical results

Finally, we numerically verify all these analytical results of Figs. 2(a)–2(c). The numerical analysis also uncovers quasiperiodic and nonstationary collective behaviors in the multistable region. In Fig. 3, we show some examples of incoherent and coherent states from multistable and stable regions. In Fig. 4, we show an example of partially coherent or cluster state from the system with clustered initial conditions. The temporal behavior of the system in this cluster state is nonstationary and the trajectory resembles a quasiperiodic orbit with multifrequency spectra. In Fig. 5, we show that the system can undergo abrupt transitions to or out of synchrony with hysteresis effects. We further uncover that the temporal behavior near the transition can become nonstationary and the trajectory can resemble quasiperiodic with multifrequency spectra. The consequence of the existence of stable coherent and stable incoherent states in the multistable region (cyan

shaded region in Fig. 2) seems to allow for a partially coherent state with complex dynamical behaviors.

III. CONCLUSIONS AND DISCUSSION

We generalized the Kuramoto model of globally coupled phase oscillators with time-delayed positive-negative coupling. We have analytically and numerically studied the stability of coherent and incoherent states in this generalized Kuramoto model. We derive the exact solutions for the critical coupling strengths at different time delays for stable incoherent and coherent states. These derivations provide insights into how the interplay of time delays can affect collective synchronization in cases of symmetric and asymmetric delays between excitatory and inhibitory oscillators. We find that fully coherent, incoherent, and multistable mixed (coherent, partially coherent, incoherent) states with hysteresis effects are possible dependent on the parameters in this generalized model. Time-delayed interactions are overall helpful for achieving synchronization in case of dominant negative coupling. The stable region of the incoherent state becomes progressively smaller and smaller with increasing delay; the area of the parameter space for the incoherent state and partially coherent state decreases at a rate of inverse of time delay. These results also suggest that delay effects can become more significant [see the peaks of Figs. 2(a)–2(c)] for delays near half the period of the oscillation or its multiples when delays are in positive couplings [Figs. 2(a) and 2(b)] and near the full period or its multiples when delays are only in negative couplings [Fig. 2(c)]. Our numerical analysis also uncovers that partially coherent or clustered states have quasiperiodic and nonstationary collective behaviors near the instability-stability boundaries. Previous studies extensively investigated the effects of time-delayed coupling [8,9] and positive-negative coupling [5,10,11] separately in the dynamics of coupled Kuramoto oscillators. We have combined these coupling schemes and obtained similar and unique analytical results. The unique analytical results include that multistable mixed states with hysteresis effects are possible in this system and that a time delay in the negative coupling increases the region of parameter space for a stable coherent state in a strongly dominant negative coupling. We expect that our work will be useful in trying to understand the role of excitation-inhibition in self-organized realistic oscillator systems, like the neuronal networks in the brain, where time delays in neuronal processing and axonal conduction of action potentials are inevitable and can vary with axonal sizes and conditions during neurodevelopment, neuroplasticity, aging, and neurodegeneration [30].

[1] Y. Kuramoto, in *Proceedings of the International Symposium on Mathematical Problems in Theoretical Physics*, edited by H. Araki, Lecture Notes in Physics Vol. 39 (Springer, Berlin, 1975); *Chemical Oscillations, Waves, and Turbulence* (Springer, Berlin, 1984).

[2] A. T. Winfree, J. Theor. Biol. **16**, 15 (1967).

[3] A. Pikovsky, M. Rosenblum, and J. Kurths, *Synchronization: A Universal Concept in Nonlinear Sciences* (Cambridge University Press, Cambridge, England, 2001).

[4] S. Strogatz, *Sync: The Emerging Science of Spontaneous Order* (Hyperion, New York, 2003).

[5] F. A. Rodrigues, T. K. DM. Peron, P. Ji, and J. Kurths, Phys. Rep. **610**, 1 (2016).

[6] S. Boccaletti, J. A. Almendral, S. Guan, I. Leyva, Z. Liu, I. Sendina-Nadal, Z. Wang, and Y. Zou, Phys. Rep. **660**, 1 (2016).

[7] P. Bak, *How Nature Works: The Science of Self-Organized Criticality* (Springer-Verlag, New York, 1996).

[8] M. K. Stephen Yeung and S. H. Strogatz, Phys. Rev. Lett. **82**, 648 (1999).

[9] M. G. Earl and S. H. Strogatz, Phys. Rev. E **67**, 036204 (2003).

[10] H. Hong and S. H. Strogatz, Phys. Rev. Lett. **106**, 054102 (2011).

[11] H. Hong and S. H. Strogatz, Phys. Rev. E **84**, 046202 (2011).

[12] T. Qui, S. Boccaletti, I. Bonamassa, Y. Zou, J. Zhou, Z. Liu, and S. Guan, Sci. Rep. **6**, 36713 (2016).

[13] Y. Maistrenko, B. Penkovsky, and M. Rosenblum, Phys. Rev. E **89**, 060901(R) (2014).

[14] S. Petkoski, J. M. Palva, and V. K. Jirsa, PLoS Comput. Biol. **14**, e1006160 (2018).

[15] H. R. Wilson and J. D. Cowan, Biophys. J. **12**, 1 (1972).

[16] X. J. Wang and G. Buzsáki, J. Neurosci. **16**, 6402 (1996).

[17] N. Brunel and X. J. Wang, J. Neurophysiol. **90**, 415 (2003).

[18] G. Buzsaki, *Rhythms of the Brain* (Oxford University Press, Cambridge, England, 2006).

[19] E. O. Mann and I. Mody, Nat. Neurosci. **13**, 205 (2010).

[20] R. A. Stefanaescu and V. K. Jirsa, PLoS Comput. Biol. **4**, e1000219 (2008).

[21] V. K. Vanag and I. R. Epstein, Phys. Rev. E **84**, 066209 (2011).

[22] S. Galam, Physica A (Amsterdam) **333**, 453 (2004).

[23] M. S. Lama, J. M. Lopez, and H. S. Wio, Europhys. Lett. **72**, 851 (2005).

[24] E. M. Izhikevich, Neural Comput. **18**, 245 (2006).

[25] B. M. Adhikari, A. Prasad, and M. Dhamala, Chaos **21**, 023116 (2011).

[26] M. Dhamala, V. K. Jirsa, and M. Ding, Phys. Rev. Lett. **92**, 074104 (2004).

[27] X. Liang, M. Tang, M. Dhamala, and Z. Liu, Phys. Rev. E **80**, 066202 (2009).

[28] V. P. Pastore, P. Massobrio, A. Godjoski, and S. Martinoia, PLoS Comput. Biol. **14**, 31006381 (2018).

[29] M. G. Rosenblum and A. S. Pikovsky, Phys. Rev. Lett. **92**, 114102 (2004).

[30] H. A. Swadlow and S. G. Waxman, Scholarpedia **7**, 1451 (2012).